Seismic Hazard Analysis of Dam Siyaho in South Khorasan province (Eastern Iran)

Malihe Baghbani[1], Ebrahim Gholami[1], Hamid Reza Rostami Barani[1]

1- Department of Geology, Tectonic, Faculty of Sciences, Birjand Branch, University of Birjand, Birjand, Iran.

* Corresponding Author: m.baghbani@birjand.ac.ir

Received: 19 July 2016 / Accepted: 05 November 2016 / Published online: 19 November 2016

Abstract

The identification of natural hazard prone areas for future planning requires an efficient decision support tool to provide the appropriate weights for the various topographical, geological, and seismological factors responsible for the expected hazards. In the present study, an analytical hierarchy process (AHP) with six earthquake hazard parameters (EHPs) was used as a decision support system for the identification of earthquake triggered hazards in the Dam Siyaho region of the South Khorasan province (Eastern Iran). The pairwise comparison matrix and the final weights for all the EHPs during the implementation of AHP were calculated with an acceptable limit of consistency ratio. A GIS-based integrated analysis was carried out on all the selected attributes to generate the final hazard and microzonation map. From the analysis, it was observed that 10.21 % of the region falls under a very high or high hazard category. The very high seismic hazard zone is located in the south region of case study, while the eastern and northwestern regions show low to very low hazard. The result of the study may be used as a first-level hazard and reliability map in selecting the appropriate earthquake resistant sites in designing the forthcoming new buildings against the potential seismic hazard of the case study.

Keywords: Seismic microzonation; Seismic hazard; GIS; Dam Siyaho; South Khorasan province; Iran.

1- Introduction

The Iranian plateau is located between two plates of Eurasia and Arabia as a part of the Alpine–Himalayan orogenic belt and is among the world's most active seismic areas. Tectonic activities in this scope are the result of northward Arabian plate movement towards Eurasia and reveal the convergence of these two plates (Berberian, 1981; Hessami *et al*., 2006; Allen *et al*., 2004). GPS studies show that the Arabian plate is moving about from 21 to 25mm northward each year (Sella *et al*., 2002; Vernant *et al*., 2004). The result of this movement on the Iranian plateau is varied due to the existence of different geological structures in different locations (Hessami *et al*., 2006), such that the amount of movement is up to 18mm per year in the Makran subduction zone and 8mm in Koppeh Dagh. There are also westward movements of about 8mm per year in the Zagros and Alborz mountains (Fu *et al*., 2007). These overall earthquakes have created heavy physical and financial damages to the area. An example is the Bam earthquake (2003, Mw: 6.6) which left over 30 000 killed, 10 000 injured, 100 000 homeless and devastated more than 80% of houses (National Report of the Islamic Republic of Iran on Disaster Reduction, 2005). Statistically, it can also be stated that during the last 100 years, the Iranian plateau has experienced 14 major earthquakes with the magnitude of 7 (on Richter scale) and 51 earthquakes with the magnitude of 6 to 7.

Earthquakes in Buin-Zahra (1962, Ms: 7.3), Dashte Bayaz (1968, Ms: 7.3), Tabas (1978, Ms: 7.8), Sirch (1981, Ms: 7.3) and Manjil (1990, Ms: 7.7) are some such examples (Mahdi and Mahdi, 2013).

Since several factors determine the seismic vulnerability of a city and all of them have to be studied simultaneously, multi-criteria decision-making (MCDM) techniques can be used in order to fill this gap. MCDM follows a collection of methods through which techniques and algorithms utilized to solve complex decision-making covering a wide range of choices and assessed by multiple, conflicting and incommensurable criteria as well as developing, assessing and prioritizing of decision-making alternatives can be used (Malczewski, 1999; Suárez-Vega *et al*., 2011). Since geographical information system (GIS) facilitates vulnerability studies and natural hazards analysis as a useful tool for managing, controlling, processing and analyzing the spatial data (Rashed and Weeks, 2003; Gamper *et al*., 2006; Almasri, 2008), utilizing GIS-based multi-criteria decisionmaking (GIS-MCDM) developed by Malczewski (2006) provides the possibility of prioritizing and combining the spatial criteria from different location and description viewpoints and eventually making comprehensive decisions. Different GIS-MCDM techniques are available depending on the required operations in order to acquire the final assessment from alternative solutions; analytic hierarchy process (AHP) is one of them.

AHP is one of the most comprehensive algorithms developed for decision-making with multi-criteria because it allows for hierarchically formulizing the complex problems; there is also the possibility of considering different quality and quantity criteria simultaneously (Chen *et al*., 2008). Thus, for solving complex spatial problems the combination of AHP with GIS resolves many issues. As a result, a great body of research has been conducted to assess the vulnerability of cities to natural events including earthquake via AHP and GIS, among which Chen *et al*. (2001), Rashed and Weeks (2003), Cutter *et al*. (2003), Servi (2004), Ebert *et al*. (2009), Schmidtlein *et al*. (2008), Botero Fernández (2009) and Nefeslioglu *et al*. (2013) are only examples.

2- Preparation of Hazard Map

The hazard maps should include information on the nature of the hazard (e.g. frequency and severity, topographical data, etc.), exposure inventory (e.g. population, buildings, highway, etc.), and the vulnerability of exposures to hazards (dense population, poorly designed buildings, low grade settlements, inadequate emergency response capacity, etc.). This combination of hazard, exposure, and vulnerability combines to define the nature of risk. There are a different ways to reveal earthquake shaking hazards and the severity of shaking and disaster triggered by it in a specific area. There are various application of an accurate hazard map like deciding insurance rates, business and land-use planning, estimations of stability and landslide potentials of hillsides, allocation planning of funds for education and preparedness for concerned general public and society. The hazard map will reduce geo-disasters impact and improve the relationships between geoenvironment and society (Wang, 2014). The United States Geological Survey (USGS, 2014) shows many parameters while preparing any seismic hazard map for a particular region of study which includes historical earthquake data, quaternary faults, crustal deformation, strong motion data, etc. Generally, seismic hazard map does not contain information about exposure inventory and vulnerability. Such information is considered in estimation and mapping of Seismic Risk. Seismic Risk is the probability of different levels of economic, social and environmental consequences of hazardous events that may occur in a specified period of time.

Since our study is limited to a unique area of Dam Siyaho in South Khorasan province (Eastern Iran) so we have included only 6 main factors which have a major impact on our study region.

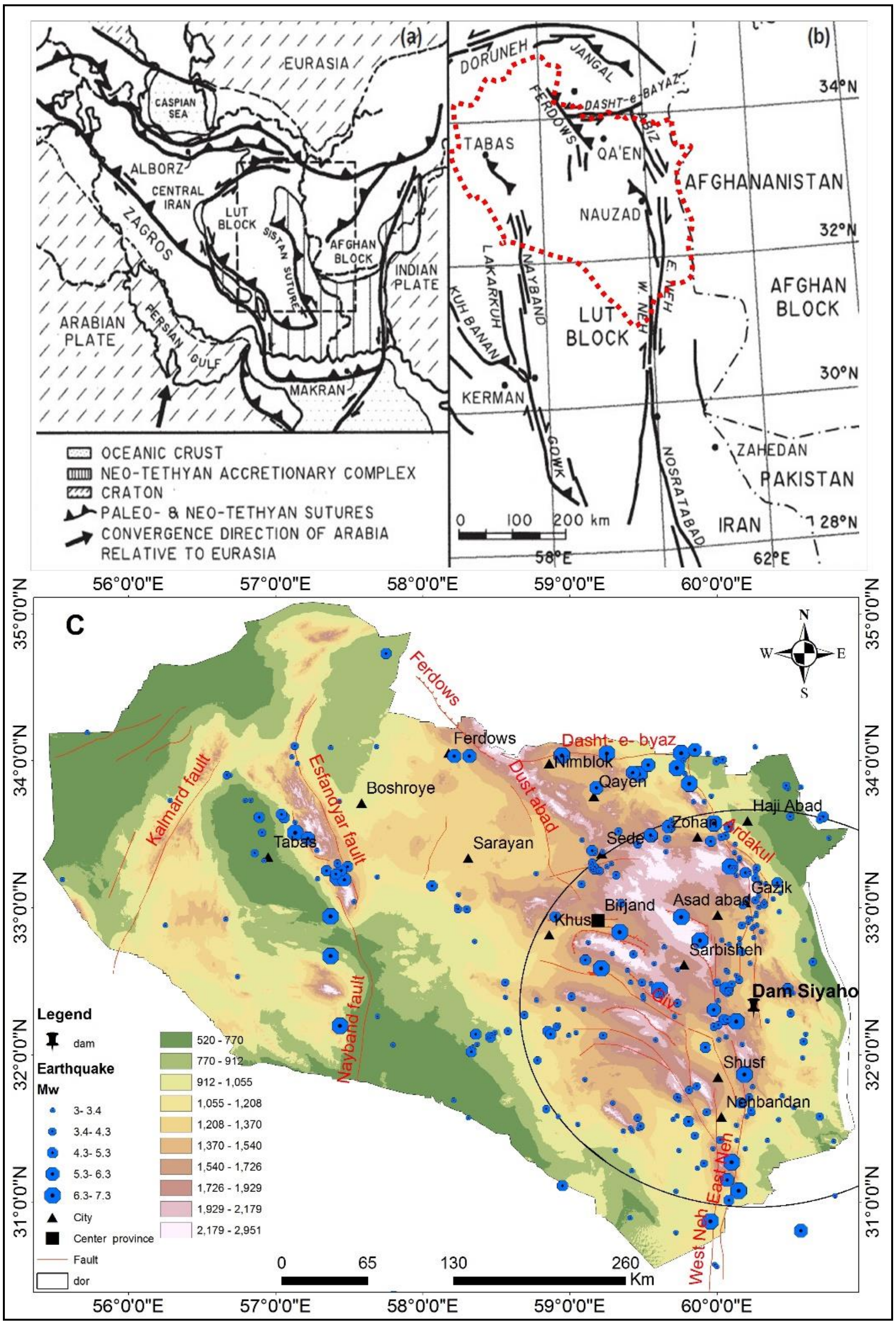

Figure 1a) The main geological units of Iran, showing the setting of the Sistan suture zone between the Afghan and Lut blocks. b) Summary map of the faulting in the Sistan suture zone (area outlined in dashed box in a (Red area: South Khorasan province). c) Location maps showing the main faults, earthquakes centers, geological and tectonic setting of the Dam Siyaho in South Khorasan province (Eastern Iran).

the main input data for estimation of the seismic hazard are: seismic source zones (active faults or areal sources) together with characteristics of possible earthquakes (maximum magnitude assigned to the zone, type of the fault, earthquake source depth, earthquake recurrence, etc.); relationships between ground-motion parameters and earthquake characteristics (e.g., ground-motion prediction equations, GMPE), information about local geological conditions. For that we have included these particular parameters for our research in Dam Siyaho scenario.

3- The study area

Dam Siyaho refers to a part of East South Khorasan province (Eastern Iran), which is located in 610 15/E and 320 01/N. The study area is located in the North part of the Sistan suture zone (Takin, 1972) (Fig. 1 a,c). The paleogeographic and tectonic evolution of Iran was presented in detail by Stöcklin (1968), Berberian and King, (1981), Ramezani and Tucker, (2003), and McQuarrie *et al*. (2003). Here, we provide a brief summary of these studies. As part of the Alpine–Himalayan orogenic system, Iran consists of a tectonic collage of Gondwana-derived terranes, which are in part separated by narrow belts of ophiolitic rocks to date (Ghazi *et al*., 2004), that had been successively accreted to the southern margin of Eurasia (Dewey *et al*., 1973; Şengör and Natal'in, 1996; Şengör *et al*., 1988). The terrane collision resulted in the development of mountain ranges, with an average elevation of ~1000−1500 m, which can be divided into three main segments: (i) the Alborz–Kopeh Dagh ranges in northern Iran, (ii) the Zagros fold and thrust belt and the Sanandaj–Sirjan structural zone (SSZ) in southwestern Iran, and (iii) the east Iranian ranges. The mountain ranges are juxtaposed with major suture zones (Fig. 1, b). A Paleotethyan suture is considered to exist along the Alborz–Kopeh Dagh ranges (Alavi *et al*., 1997), whereas the Bitlis– Zagros suture in southwestern Iran (Agard *et al*., 2011 and references therein) and the Sistan suture in eastern Iran (McCall, 1997; Tirrul *et al*., 1983) are considered Neotethyan in origin. Surrounded by these mountain ranges is a region of moderate relief known as the central Iranian microcontinent containing the Lut, Tabas and Yazd blocks from east to west (Fig. 1 b). Northward subduction of the Gulf of Oman beneath southern Iran is currently active (McCall, 1997).

4- Materials and methods

The materials used in the present study are remote sensing data, geo-reference data, tabular or descriptive data and filed data. All collected or estimated data are combined in a geo-spatial database on the ArcGIS platform.

4.1- Database

To assess the seismic hazards in the study area, the geomorphological, geological, and geographical parameters are each taken into consideration, in conjunction with the record of the seismic activities that have affected Dam Siyaho region of the South Khorasan province (Eastern Iran). Historical seismic events could not be included due to insufficient reports and catalogs.

An area with a 150 km radius centered at Dam Siyaho was selected to determine the preliminary seismic hazard regions using the AHP method on GIS platform. In the present study, six different factors were computed covering Seismic moment, surface PGA, and Energy. An extensive geodatabase has been developed in the GIS platform using Fault Density, Distance to Fault, Lithology and remote sensing data.

The seismotectonic map was adopted from the published geological faults (Iranian Seismological Center). The topography of the area was extracted from the digital elevation model (DEM) with a 30 m resolution. The DEM was acquired from the advanced spaceborne thermal emission and reflection radiometer global digital elevation model (ASTER GDEM) (Aster 2009, 2011). Earthquake epicenters were collected from the International Seismological Centre (ISC) (ISC 2014)) for the period between

1965 and 2014. Faults were digitized from the geological maps of Dam Siyaho quadrangles (Iranian Seismological Center). Publicly available LANDSAT 5TM/7ETM satellite images recorded in 2005 were also used for the determination of surface lineaments (Markham and Barker 1986; Kamel 1991; Masoud and Koike 2006; Hashim *et al*. 2013). The selection of the appropriate factors and the determination of the classes, as well as their boundary values, was based on an extensive literature review (e.g., Nath 2004, 2005; Kienzle *et al*. 2006; Mohanty *et al*. 2007; Parolai *et al*. 2007; Mohanty and Walling 2008; Nath *et al*. 2008; Papadimitriou *et al*. 2008; Nath and Thingbaijam 2009; Ganapathy 2011; Erol and Topal 2013; Grasso and Maugeri 2012; Turk *et al*. 2012; Quadrio *et al*. 2015) and personal experience.

4.1.1- Seismic Moment and Energy

The size of an earthquake can be express by the released energy. The energy carried by seismic waves is proportional to the square of their amplitude and, thus, magnitude is proportional to the logarithm of the energy. Gutenberg and Richter (1956) established the first empirical relation between the magnitude and energy:

$$LogE = 5.8 + 2.4 m_b \quad (1$$

$$LogE = 11.8 + 1.5 m_s \quad (2$$

Obviously these relationships are affected by the problem of saturation said in the previous paragraph. Another measure of the size of an earthquake is the seismic moment M0, which was introduced by Aki (1966). It is based on the idea that earthquakes are caused by a shear fracture in the Earth's crust and is defined as:

$$M_0 = \mu AD \quad (3$$

where y is the shear modulus, *D* is the mean slip on the fault and *A* is the area of the ruptured fault plane. The seismic moment thus constitutes a good physical measure of the size of an earthquake closely linked to the source. Following Kostrov (1974):

$$E_s \approx \frac{1}{2} \Delta\sigma.\mathrm{D.A} \quad (4$$

Using the seismic moment definition:

$$E_s \approx \frac{\Delta\sigma}{2\mu} M_0 \quad (5$$

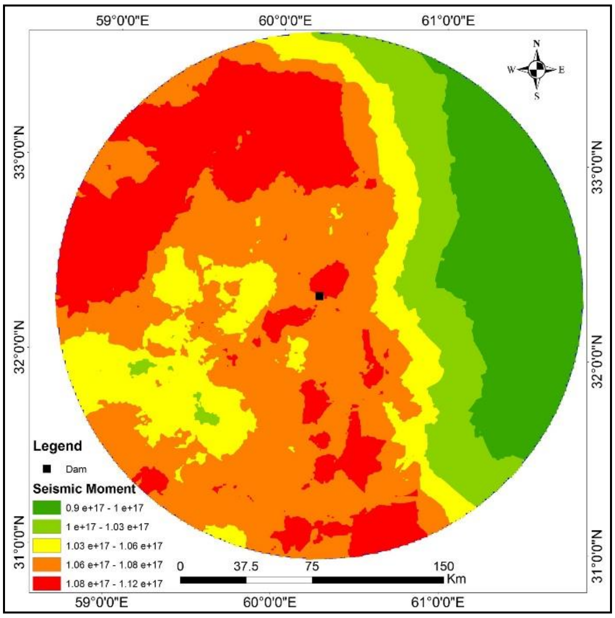

Figure 2) Seismic Moment map of Dam Siyaho in South Khorasan province (East Iran).

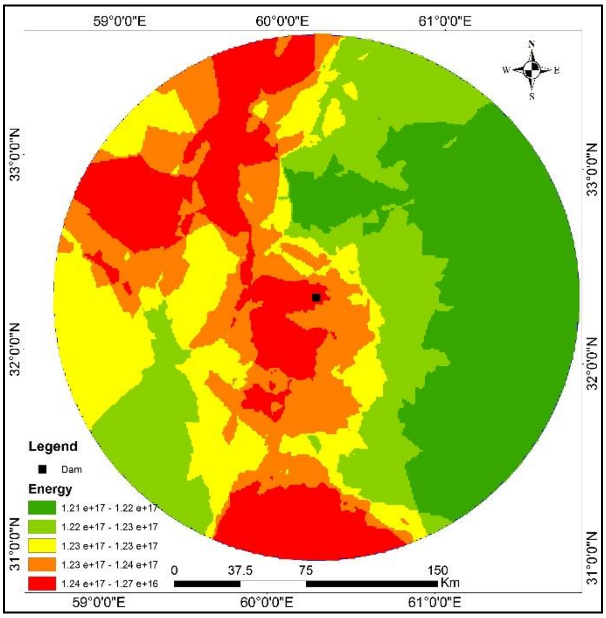

Figure 3) Energy map of Dam Siyaho of South Khorasan province (East Iran).

This expression relates the total energy released by an earthquake to its seismic moment and stress drop.

Kanamori (1977) proposed a new scale, called moment magnitude Mw that does not saturate even at high magnitudes. Assuming a constant value for the stress drop such that $10^{-4} \approx \frac{\Delta\sigma}{\mu}$ the relation (6) becomes:

$$E_s \approx \frac{2M_0}{10^4} \quad (6$$

Substituting in (8)

$$LogM_0 \approx 1.5M_s + 16.1 \quad (7$$

From this relationship we obtained the definition of the moment magnitude in terms of the seismic moment:

$$M_w = \frac{2}{3}(Log M_0 - 9.1) = \frac{2}{3} Log M_0 - 6.1 \quad (8$$

Using formulas 1 to 8, the seismic moment and seismic energy for each area were calculated. Using GIS software cumulative seismic moment and the energy map of the region were prepared. In conclusion the moment magnitude can be considered the best measure of the size of an earthquake being linked to the seismic moment (that for a tectonic event assumes the mechanism of shear fracture, Figs. 2 and 3). In Figures 2 and 3, the cumulative plans for the torque and power of an earthquake in the region are shown. In the areas large earthquakes occurred in torque and high energy seismic. In the Northeast amount of torque and power are high.

4.1.2- Peak ground acceleration (PGA)

Peak Ground Accelerations (PGA) is the parameter which is referred to the attenuation seismic wave's characteristics of a region. Earthquake resistant designing of structures and facilities involves the estimation of ground shaking level, which they will experience thereafter. Since the level of shaking is most conviently illustrated by ground motion parameters, thus the methods to estimate the ground motion parameters are utilized. Predictive relationships, which express a particular ground motion parameter in terms of the quantities that affect it most strongly, are used for this purpose. Predictive relationships have a significant role in conducting seismic hazard analyses (Kramer, 1996).

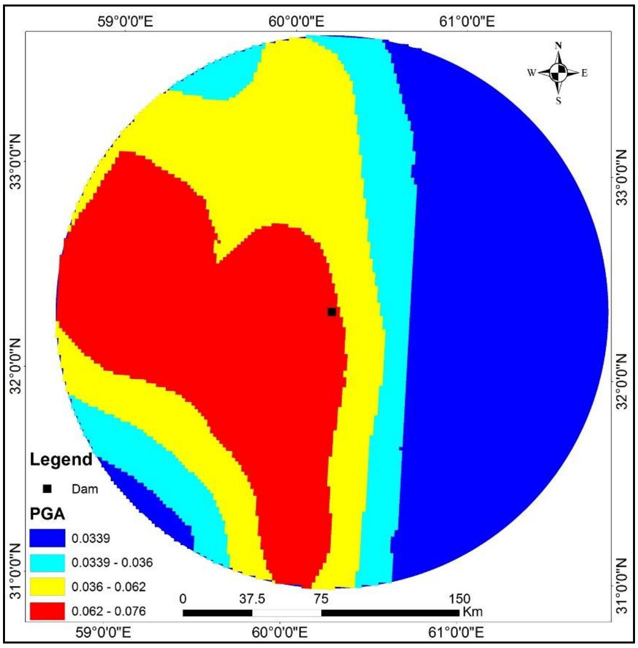

Figure 4) PGA index map of the study area.

The acceleration due to strong ground motion at each site depends on a complex combination of the earthquake's magnitude, duration, frequency content, the distance between the earthquake's hypocenter and site, soil condition in the scope, etc. Thus, one of the important criteria while designing the structures, and also one of the main reasons for the building damages, is the peak ground acceleration (PGA) while an earthquake occurs (Ghodrati Amiri *et al*., 2010; Babayev *et al*., 2010; Arma¸s, 2012; Moradi *et al*., 2013; Panahi *et al*., 2014). In Iran, the peak ground acceleration which had destroyed or damaged the structures was 0.1 g (during the Golbaf earthquake in 1981) and about 0.989 g during the Zanjiran (1994) and Bam (2003) earthquakes (Jafargandomi *et al*., 2004).

This plan is consistent with Map cumulative seismic moment and energy. Map cumulative seismic moment and the energy in the highest torque and power in central and northeast. As a result of seismic activity and quaternary faults in this section appears.

In this study, the Peak Ground Accelerations (PGA) was classified into five classes. The low and very low Peak Ground Accelerations (PGA is scattered in the northwest and central part of the study area (Fig. 4).

4.1.3- Fault Density (FD) and Distance to Fault (DF)

The fault is linear feature on the Earth's surface that reflects a general surface expression of underground Fractures (Pradhan *et al*., 2006; Pradhan and Youssef, 2010). Most earthquakes occur near active faults. Areas near fault lines have a higher risk of earthquakes. The higher the concentration of active faults in the region, the greater the probability of earthquakes in that area more. They are categorized as the secondary porosity and visible on satellite images as tonal differences compared to other terrain features. Faults of the area were extracted from the Landsat ETM+ image using Sobel directional filtering and high-pass directional filtering (Pradhan and Pirasteh, 2010). The concentration of Faults is more in the central and west part of the study area. In a similar manner to the drainage density, the Fault density (Fd) was calculated based on the mesh network method. The Fd was defined as the total length of all recorded Faults divided by the area under consideration (Edet *et al*., 1998). This is shown in the following equation:

$$Dd = \sum_{i=1}^{i=n} \frac{F}{A} (km^{-1}) \qquad (9$$

Where ΣF is the total length of all Fault (km) and A is the area of the grid (km^2). In this study, the Fault density was classified into five classes: <0.019 km/km^2 (very low), 0.019–0.026 km/km^2 (low), 0.026–0.034 km/km^2 (moderate), 0.034–0.041 km/km^2 (high), and 0.041–0.049 km/km^2 (very high) (Fig. 5).

4.1.4- Lithology

Lithology is among the most significant parameters for seismic hazards (Moustafa *et al*., 2016). The lithology layer was prepared by digitizing the geological map (Geological Survey Department of Iran) (Fig. 7).

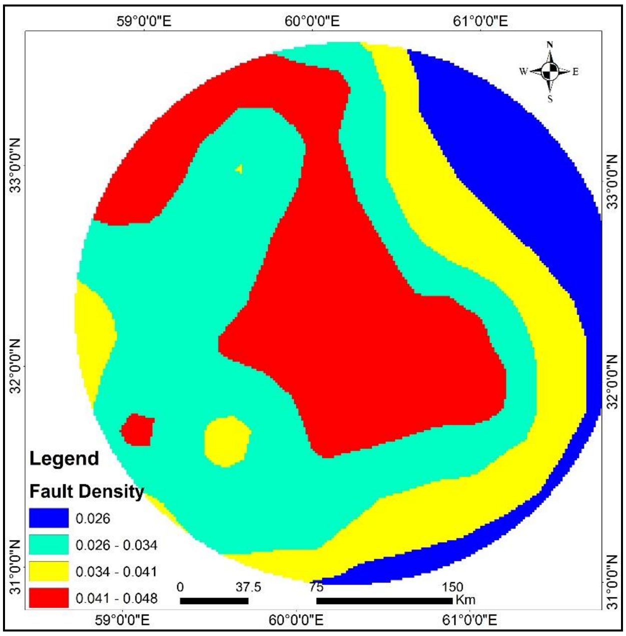

Figure 5) Fault density index map of the study area.

In this study, the Distance to Fault was classified into five classes: >4000 m (very low), 3000-2000 m (low), 2000-1000m (moderate), 1000-500 m (high), and 0-500 m (very high) (Fig. 6).

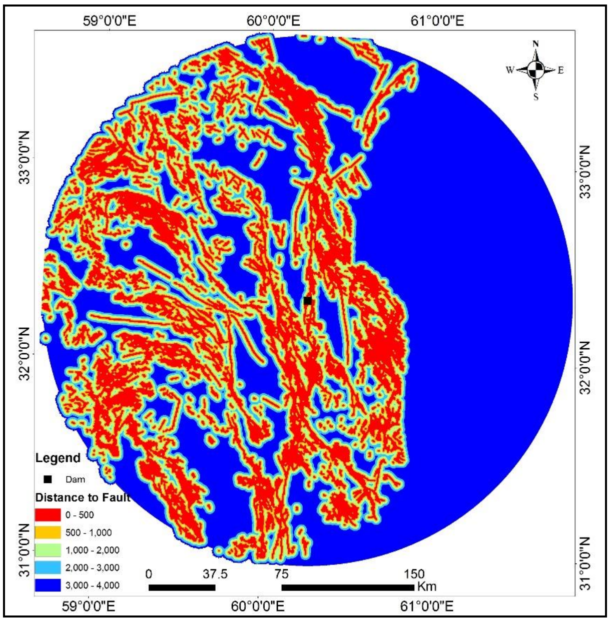

Figure 6) Distance to Fault index map of the study area.

The lithology of the study area consists mainly of quaternary alluvial, diorite, and diorite–gabbro rocks. The east Iranian ranges and the Sistan suture zone mark the closure of the Sistan

Ocean, a narrow branch of Neotethys that opened during the Middle Cretaceous (Camp and Griffis, 1982; Tirrul *et al*., 1983). This was accompanied by the suturing between the Lut block and the Afghan block to the east at the Late Cretaceous (Saccani *et al*., 2010; Zarrinkoub *et al*., 2010). Magmatism for the Lut block was active from the Jurassic to Quaternary with a dominant pulse during the Eocene– Oligocene (see Karimpour *et al*., 2011 for review), which resulted in calc-alkaline rocks covering a region of at least ~300×400 km^2. The Late Cenozoic alkali basalts crop out along the Neh faults in the Sistan suture zone, eastern Iran. The faults represent two active, N–S-trending dextral strike–slip fault systems separated by a distance of ~5 km largely covered by a desert (*i.e.* Dasht-e–Lut) (Wellman, 1966; Walker and Jackson, 2002).

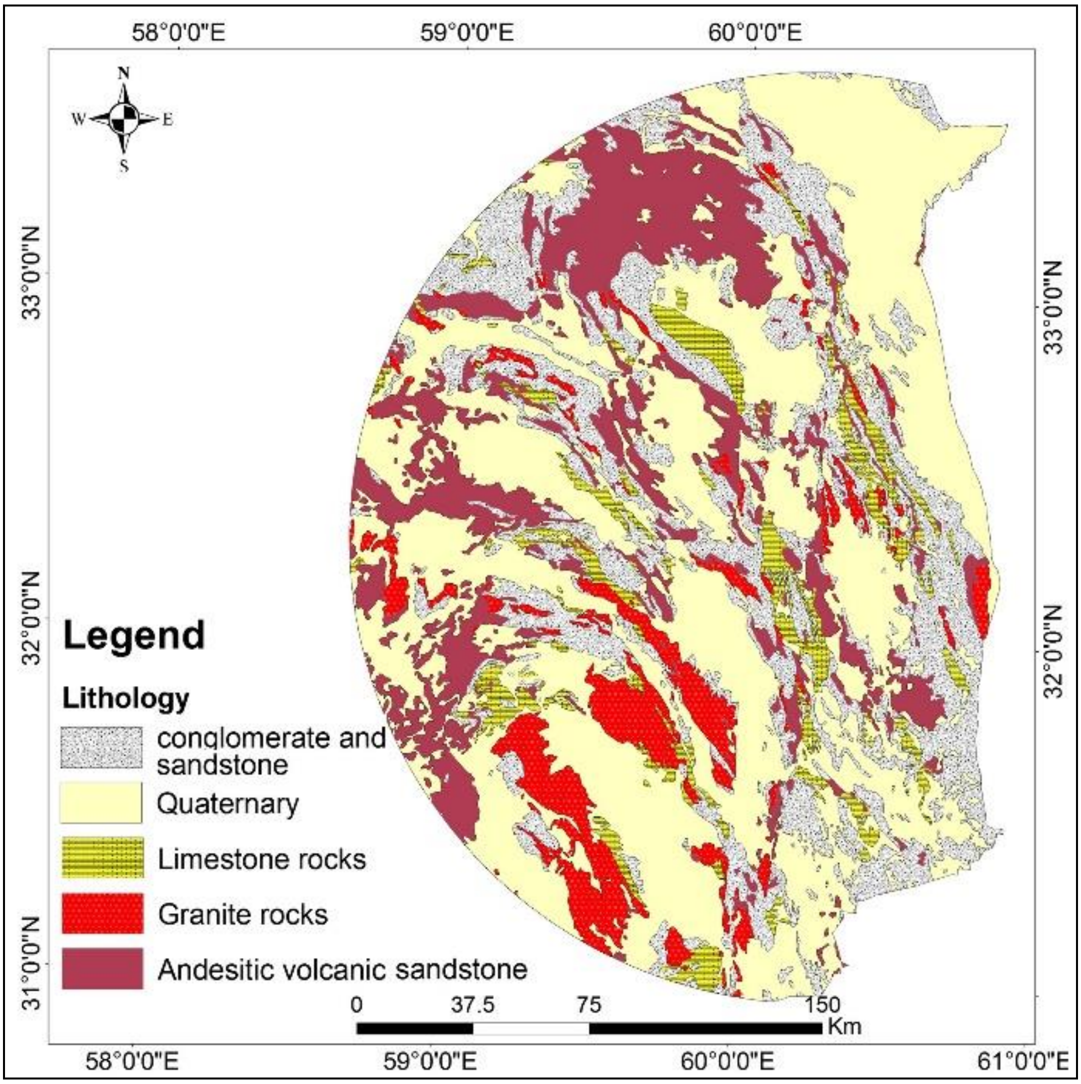

Figure. 7) Map showing the study area location and geology.

5- Methodology for prioritization using AHP

The multi-criteria AHP evaluation technique was adopted for the microzonation mapping (Saaty 1994, 2008). This technique uses a hierarchical structure through pairwise comparison based on a judgment between two particular hazard elements rather than seeking to prioritize an entire list of hazardous constituents (Estoque 2012). In this way, a matrix (A = [aij]) of pairwise comparisons between the selected seismic hazard factors can be constructed, based on Saaty’s (2008) predefined scale, in a procedure of allocating weights in the participatory mode. For the computation of the pairwise comparison matrix, where each entry represents the relative significance of a factor to the others, the relative importance between two factors was measured according to a numerical scale from one to nine, as given in (Saaty 1988). The value one means equal importance, and the value nine means extreme importance.

Inversely, less important variables were rated between 1 and 1/9 (Saaty 1988, 1990). The various characteristics of the considered hazard thematic layers are then assigned a score, also normalized to assure that no layer exerts an influence beyond its limited weight (Saaty 2008). To fill the upper triangular of the pairwise comparison matrix, in each iteration two parameters are considered one by one and, considering the relative importance, a value between one and nine is assigned. The relative importance between two factors in the matrix can be filled on the basis of field experience, survey results, and the comparison guidelines presented in (Saaty 2008). The elements in the lower part of the matrix can be filled by taking the reciprocal of the corresponding elements in the upper matrix such as, if an element Aij = a, then Aji = 1/a and if i = j, then Aij = - Aji = 1. Following the construction of all pairwise comparison matrices, the weight vector w = [w_1, w_2, …, w_n]$_T$, is calculated utilizing the principal Eigenvector of the matrix. The normalized principal eigenvector, which is called the priority vector, can be used to assign the weights for the different selected EHPs. The principal eigenvalue (kmax) of the priority vector may be computed approximately by the summation of the products between each element of the eigenvector and the sum of the columns of the reciprocal matrix. The results are in the range of zero to one and their sum adds up to one in each column. Since the decisions regarding the relative importance of the utilized parameters are subjective, they will vary from person to person, and hence a consistency check is employed to assess the consistency of decisions in the AHP analysis. The consistency of judgement can be checked by estimating the consistency ratio (CR), which can be computed from the ratio of the consistency index (CI) and the random consistency index (RI). The CI is a unit-less number that depends on the size of the matrix (number of parameters) and the consistency in decisions; it can be estimated using the following equation:

$$Cl = \frac{\lambda \max - n}{n - 1} \qquad (10$$

where kmax is the principal eigenvalue obtained from the priority matrix and n is the size of the comparison matrix. At each stage of the pairwise comparison process, the CR has to be less than 0.1 for acceptable pairwise comparisons. Larger values of the CR indicate inconsistent hazard judgements, suggesting that the initial values of the pairwise comparison matrix need to be revised (Estoque, 2012). Since EHPs vary significantly and depend on several factors, they need to be classified into various ranges, which are known as the features of the utilized thematic layer.

Hence, each EHP's feature is rated or scored within EHPs and then this rate is normalized. A raw rating for each feature of the various EHPs is, therefore, allocated initially on a standard scale, such as 1–10 and then normalized using the relation,

$$Xi = \frac{Ri - R\min}{R\max - R\min} \qquad (11$$

where *Xi* is the normalized rate; Ri is the rating assigned to the features within a single EHP, and Rmin and Rmax are the minimum and maximum rates of a particular EHP (Estoque, 2012; Fig. 8, Table 1).

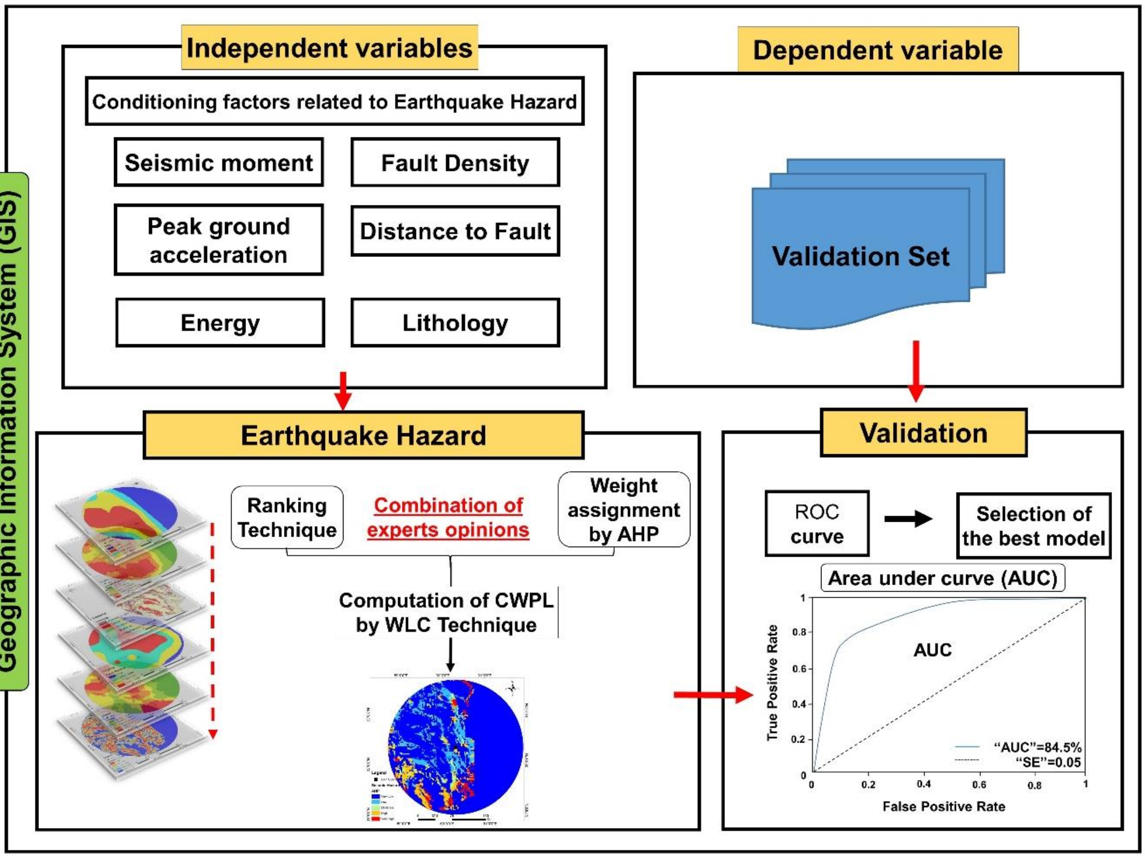

Figure 8) Flowchart showing the methodology adopted in this study.

Table 1) Pair-wise comparison matrix for the AHP process in Dam Siyaho region of the South Khorasan province (Eastern Iran).

layer	Expert weights	SM	PGA	En	FD	DF	L
SM	0.381	1	2	3	4	5	7
PGA	0.25	2	1	2	3	4	6
E	0.153	3	2	1	2	3	5
L	0.101	4	3	2	1	2	4
FD	0.071	5	4	3	2	1	3
DF	0.043	7	6	5	4	3	1

Consistency ratio (CR) =0.07<0.1

6- Criteria selection and analysis

The evolution of the different thematic layers for earthquake hazards is mainly divided into geological and seismological principal attributes (Pal *et al*., 2008) to accommodate for all potential sources of geohazards in the mapped region. The geological attributes, such as geological parameters (L), Fault Density (FD) and Distance to Fault (DF) are considered. The Seismic moment (SM), Peak ground acceleration (PGA) and Energy (E) are also considered as seismological attributes. Fig 8 illustrates the methodological flowchart adopted for the generation of the first level microzonation map. L, FD, DF, SM, PGA and E thematic layers were used to incorporate in the AHP and they are associated with the earthquake hazard.

Relational analysis was carried out to classify each triggering hazard attribute into several classes. First, the hazard area of a particular class of each of the triggering factor maps was determined by using the zonal histogram function in the ArcGIS 10.0 spatial analyst tool. The proportions of the area covered by each class of the different hazard layers were computed and a subjective relational analysis between the computed proportion and the factorization classes were carried out. The actual priority rank of the various triggering factors was subsequently calculated from the relation between the vector classes and the percentages of the area covered by that class. The calculated classes of the various triggering factors were then used for further AHP analysis.

An important constraint in the evaluation is the rating of the classes of each parameter involved in the analysis. In the present study, each attribute layer is classified based on their relative contribution towards the final hazard micro zonation map. The map of each thematic layer was classified. Ranks assigned to different features of the individual themes and their normalized weights are presented in Table 2 (Machiwal *et al*., 2011; Chowdary *et al*., 2013).

7- Normalized weights of different features of thematic layers

Table 2) Assigned and normalized weights of different features of 6 thematic layers for Seismic Hazard.

Factor	Class	Assigned rank	Feature normalized ranks (Nr)
Seismic moment (SM)	1.21e+17 - 1.23e+17	1	0.381
	1.23e+17 - 1.24e+17	2	
	1.24e+17 - 1.25e+17	3	
	1.25e+17 - 1.26e+17	4	
	1.26e+17 - 1.3e+17	5	
Peak ground acceleration (PGA)	<0.0339	1	0.25
	0.0339 - 0.036	2	
	0.036 - 0.062	3	
	0.062 - 0.068	4	
	0.068 - 0.076	5	
Energy (En)	2.076e+17 - 2.136e+17	1	0.153
	2.136e+17 - 2.21e+17	2	
	2.21e+17 - 2.23e+17	3	
	2.23e+17 - 2.4e+17	4	
	2.4e+17 - 2.45e+17	5	
Lithology (L)	Andesitic, Rhyolitic, Deictic, Basaltic, Diabase	1	0.101
	Granite, Gabbro, Diorite, Metamorphic	2	
	Sandstone, Limestone &Conglomerate	3	
	Shale&Marl	4	
	Quaternary	5	
Fault Density (FD)	<0.019	1	0.071
	0.019-0.026	2	
	0.026-0.034	3	
	0.034-0.041	4	
	0.041-0.049	5	
Distance to Fault (DF)	>2000	1	0.043
	1500-2000	2	
	1000-1500	3	
	500-1000	4	
	0-500	5	

8- Validation of Seismic Hazard map

Validation is the most important process of modeling in that without validation, the models will have no Scienceentific significance (ChungJ and Fabbri, 2003). For validation, receiver operating characteristic (ROC) analysis by comparing the existing well yield data with the groundwater potential map obtained by AHP model was used (Pradhan 2009; Mohammady *et al*. 2012; Pourghasemi *et al*., 2012; Davoodi Moghaddam *et al*., 2013; Pradhan, 2013; Regmi *et al*., 2013; Pourtaghi and Pourghasemi, 2014).

The validation curves are shown in Fig. 8. ROC plot assessment results (Fig. 9) show that in the Seismic Hazard map using AHP, the AUC was 0.845, which corresponds to the prediction accuracy of 84.5%. Therefore, it can be implied that the model utilized in this study showed reasonably good accuracy in predicting the Seismic Hazard map. Moreover, it is concluded that the AHP model can be used as a simple tool for the assessment of groundwater potential. Yalcin (2008) and Pourghasemi *et al*. (2013) stated that AHP as an expert knowledge-based model is very useful for solving complex problems. Srivastava and Bhattacharya, (2006) and Jha *et al*. (2010) demonstrated that the RS, GIS, and MCDA techniques provide a useful integrated tool for evaluating the groundwater conditions at a basin or subbasin scale. Jankowski (1995) stated that the main purpose of the AHP method is to support the decision makers in selecting the best alternative from the various possible choice alternatives under the presence of multiple priorities.

The verification of the Seismic Hazard map using yield data shows that this prediction method is effective and reliable. This result is in line with the results of Lee *et al*. (2012) that applied an artificial neural network (ANN) model and a geographic information system (GIS) to the mapping of regional groundwater productivity potential (GPP) for the area around Pohang City, Republic of Korea. The validation showed prediction accuracies between 73.54 and 80.09 %. They used the weighted overlay modeling technique to develop a groundwater potential model with eight different effective weighted thematic layers, including annual rainfall, lithology, lineament density, topography, slope, and drainage density. The groundwater potential map can be prepared based on surface thematic layers (e.g., drainage density and slope) which are easily accessible and hence are widely used (Jha *et al*., 2007; Adiat *et al*., 2012), especially in developing and low-income countries.

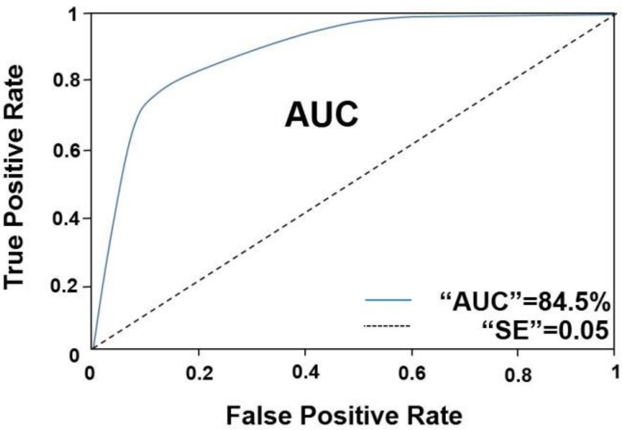

Figure 9) ROC curve for the Seismic Hazard map.

The evolution of the different layers for earthquake hazards is mainly divided into geological and seismological principal attributes (Pal *et al*. 2008) to accommodate for all potential sources of geohazards in the mapped region. The geological attributes, such as geological parameters (L), Fault Density (FD) and Distance to Fault (DF) are considered. The SM, PGA and En are also considered as seismological attributes. Figure 8 illustrates the methodological flowchart adopted for the generation of the first-level microzonation map. L, PGA, SM and EN layers were used to incorporate in the AHP and they are associated with the earthquake hazard.

Additionally, the L, FD, and DF layers they correspond to the earthquake-induced hazards. Relational analysis was carried out to classify each triggering hazard attribute into several classes. First, the hazard area of a particular class of each of the triggering factor maps was determined by using the zonal histogram function in the ArcGIS spatial analyst tool. The proportions of the area covered by each class of the different hazard layers were computed and a subjective relational analysis between the computed proportion and the factorization classes were carried out. The actual priority rank of the various triggering factors was subsequently calculated from the relation between the vector classes and the percentages of the area covered by that class. The calculated classes of the various triggering factors were then used for further AHP analysis. An important constraint in the evaluation is the rating of the classes of each parameter involved in the analysis. In the present study, each attribute layer is classified based on their relative contribution towards the final hazard micro zonation map.

9- Results and discussion

9.1- Application of AHP model for Seismic Hazard mapping

AHP is a model that has been widely used by different researchers in the field of natural resources and environmental management. The final weight of each conditioning factor was shown in Table 2. In this study, the CR is 0.07; the ratio reflects a reasonable level of consistency in the pairwise comparisons phase. The final Seismic Hazard map obtained by AHP model is shown in Figure 10. Based on this map, high Seismic Hazard zones are located at the northern, south and central of the plain. This map is the result of overlapping of all data used. This overlap of great assistance to earthquake prone areas of high and low to be detected (Heidari *et al.* 2015). This map is used as a base map for seismic studies.

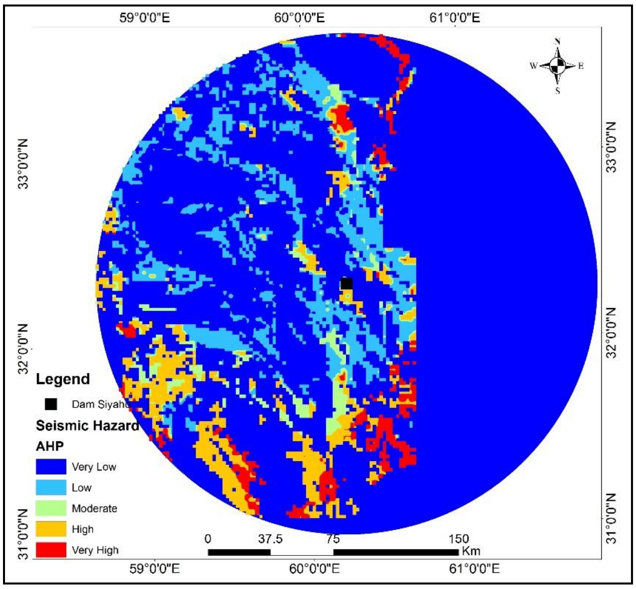

Figure 10) Seismic Hazard maps based on AHP models of Dam Siyaho region of the South Khorasan province (Eastern Iran).

The obtained pixel values was then classified based on natural break classification scheme (Pourghasemi *et al*. 2012; Regmi *et al*. 2013; Pourghasemi *et al*. 2013; Zare *et al*. 2013) into low, moderate, high, and very high potential groups. The Seismic Hazard map achieved from the AHP method, which covered 8.76 % of the total area, was designated to be a moderate SPM class; 21.6, 37.1, 22.3 and 10.21% of the total area are related to very low, low, high, and very high SHM, respectively (Fig. 10 and Table 3).

$$SHM = (SM) + (PGA) + (E) + (FD) + (DF) + (L) \quad (12$$

Table 3) The distribution of the Seismic Hazard values and areas with respect to the Seismic Hazard in Dam Siyaho region of the South Khorasan province (Eastern Iran).

SPM	Binary Index Overlay and Fuzzy logic Model	
	Area (%)	Area (km^2)
Very Low	21.6	15
Low	37.1	26
Moderate	8.76	6
High	22.3	16
Very High	10.21	7

10- Conclusions

Assess the risk of earthquakes using seismic data (1965-2016) and risk factors in the prediction of earthquakes (geological parameters (L), Fault Density (FD), Distance to Fault (DF), Seismic moment (SM), Peak ground acceleration (PGA) and Energy (E)), was conducted for the province. Based on the results of this study, the following conclusions were drawn:

1- Dam Siyaho is a case study of moderate to Moderate seismic hazard.

2- More likely seismic hazard based on the formula experimental, seismic moment and the energy associated with faults Nehbandan, Charpansar, Porang, Zolesk, Doroh, Chah Kho, Afzal Abad.

3- The very high seismic hazard zone is located in the northern, south and central region of Dam

Siyaho. While the east regions show low to very low hazard.

4- The study shows that areas near Fault are more vulnerable and the population near it is on a high risk zone.35.1 % of total study area falls under high risk zone, 8.76 % under medium risk, and 58.7 % under low risk zone.

5- The validation of results demonstrated that AHP has fairly good predication accuracy of 84.5 %. Hence, based on the results of this research and the accuracy of the derived Seismic Hazard map, it can be concluded that the applied methodology, together with the used indices, is a useful framework for the rapid assessment of Seismic Hazard and can be recommended to be applied in other areas especially in data scarce areas.

References

Adiat, K. A. N., Nawawi, M. N. M., Abdullah, K. 2012. Assessing the accuracy of GIS-based elementary multi criteria decision analysis as a spatial prediction tool a case of predicting potential zones of sustainable groundwater resources. Journal Hydrology: 440, 75–89.

Agard, P., Omrani, J., Jolivet, L., Whitechurch, H., Vrielynck, B., Spakman, W., Monié, P., Meyer, B., Wortel, R. 2011. Zagros orogeny: a subduction-dominated process. Geological Magazine: 148, 692–725.

Aki, K. 1966. Estimation of earthquake movement, released energy and stress-strain drop from G-waves spectrum. Bull Earthquake Research Institute : 44, 23–88.

Alavi, M., Vaziri, H., Seyed-Emami, K., Lasemi, Y. 1997. The Triassic and associated rocks of the Nakhlak and Aghdarband areas in central and northeastern Iran as remnants of the southern Turanian active continental margin. Geological Society of America Bulletin : 109, 1563–1575.

Allen, M., Jackson, J., Walker, R. 2001. Late Cenozoic reorganization of the Arabia-Eurasia collision and the comparison of short-term and long-term deformation rates, Tectonics: 23, 1–16.

Almasri, M. N. 2008. Assessment of intrinsic vulnerability to contamination for Gaza coastal aquifer, Palestine. Journal of Environmental Management: 88, 577–593.

Arma¸ S. I. 2012. Multi-criteria vulnerability analysis to earthquake hazard of Bucharest, Romania. Natural Hazards: 63, 1129–1156.

Aster, G. 2009. Validation Team. ASTER Global DEM validation, summary report.

Aster, G. 2011. Validation Team, 2009. ASTER Global DEM validation: summary report. METI and NASA.

Babayev, G., Ismail-Zadeh, A., Le Mouël, J. L. 2010. Scenariobased earthquake hazard and risk assessment for Baku (Azerbaijan), Nat Hazards Earth Syst Science: 10, 2697–2712.

Berberian, M., King, G. C. P. 1981. Towards a paleogeography and tectonic evolution of Iran, Can. Journal of Earth Sciences: 18, 210–265.

Botero Fernández, V. 2009. Geo-information for measuring vulnerability to earthquake: a fitness for use approach, PhD thesis, ITC. Nether. 158.

Camp, V. E., Griffis, R. J. 1982. Character, genesis and tectonic setting of igneous rocks in the Sistan suture zone, eastern Iran. Lithos: 15, 221–239.

Chen, K., Blong, R., Jacobson, C. 2001. MCE-Risk: integrating multi-criteria evolution and GIS for risk decision-making in natural hazards, Environ. Modelling and Software: 16, 387–397.

Chen, M. F., Tzeng, G. H., Ding, C. G. 2008. Combining fuzzy AHP with MDS in identifying the preference similarity of alternatives. Applied Soft Computing: 8, 110–117.

Chowdary, V. M., Chakraborthy, D., Jeyaram, A., Krishna Murthy, Y. V. N., Sharma, J. R., Dadhwal, V. K. 2013. Multi-criteria decision making approach for watershed prioritization using analytic hierarchy process technique and GIS. Water Resources Management: 27, 3555–3571.

ChungJ, F., Fabbri, A. G. 2003. Validation of spatial prediction models for landslide hazard mapping. Natural Hazards: 30, 451–472.

Cutter, S. L., Boruff, B. J., Shirley, W. L. 2003. Social vulnerability to environment hazards. Social Science Quarterly: 84, 242–261.

Davoodi Moghaddam, D., Rezaei, M., Pourghasemi, H. R., Pourtaghie, Z. S., Pradhan, B. 2013. Groundwater spring potential mapping using bivariate statistical model and GIS in the Taleghan watershed, Iran. Arabian Journal GeoScience: 8, 913–929.

Dewey, J. F., Pitman, W. C. I. I. I., Ryan, W. B. F., Bonnin, J. 1973. Plate tectonics and the evolution of the Alpine system. Geological Society of America Bulletin: 84, 3137–3180.

Ebert, A., Kerle, N., Stein, A. 2009. Urban social vulnerability assessment with physical proxies and spatial metrics derived from air- and spaceborne imagery and GIS data, Natural Hazards: 48, 275–294.

Edet, A. E., Okereke, C. S., Teme, S. C., Esu, E. O. 1998. Application of remote-sensing data to groundwater exploration: a case study of the Cross River State, southeastern Nigeria. Hydrogeological Journal: 6, 394–404.

Erol, G., Topal, T. 2013. GIS-based microzonation of the Niksar settlement area for the purpose of urban planning (Tokat, Turkey). Environmental Earth Sciences: 68, 2065–2084.

Estoque, R. C. 2012. Analytic hierarchy process in geospatial analysis. In: Progress in geospatial analysis. Springer, Japan, pp.157–181.

Fu, B., Lei, X., Hessami, K., Ninomiya, Y., Azuma, T., Kondo, H. 2007. A new fault rupture scenario for the 2003 M w 6.6 Bam earthquake, SE Iran: insights from the high-resolution Quick- Bird imagery and field observations. Journal of Geodynamics: 44, 160–172.

Gamper, C. D., Thöni, M., Weck-Hannemann, H. 2006. A conceptual approach to the use of Cost Benefit and Multi Criteria Analysis in natural hazard management. Natural Hazards and Earth System Sciences: 6, 293–302.

Ganapathy, G. P. 2011. First level seismic microzonation map of Chennai city– a GIS approach. Natural Hazards and Earth System Sciences: 11, 549–559.

Ghazi, A. M., Hassanipak, A. A., Mahoney, J. J., Duncan, R. A. 2004. Geochemical characteristics, 40Ar–39Ar ages and original tectonic setting of the Band-e-Zeyarat/Dar Anar ophiolite, Makran accretionary prism, S.E. Iran. Tectonophysics: 393,175–196.

Ghodrati Amiri, G., Kazemiashtiani, V., Razavian Amrei, S. A. 2010. Seismic hazard analysis and obtaining peak ground acceleration (PGA) for Arak Region, Iran. Asian Journal of Civil Engeering: 11, 183–206.

Grasso, S., Maugeri, M. 2012. The Seismic Microzonation of the City of Catania (Italy) for the Etna Scenario Earthquake (M = 6.2) of 20 February 1818. Earthquake Spectra: 28, 573–594.

Gutemberg, B., Richter, C. F. 1956. Magnitude and energy of earthquake. Annali di Geofisica (Rome): 9, 1–15.

Hashim, M., Ahmad, S., Johari, M. A. M., Pour, A. B. 2013. Automatic lineament extraction in a heavily vegetated region using Landsat Enhanced Thematic Mapper (ETM plus) imagery. Advances in Space Research: 51, 874–890.

Heidari Aghagol, M., Khatib M. M., Heyhat, M. R., Mansori, H. 2015. Earthquake hazard zoning of Analytical Hierarchy Process (AHP) and fuzzy logic (study area: South Khorasan province) (in Persian). Journal of Tectonic: 4, 43–63.

Hessami, K., Nilforoushan, F., Talbot, C. J. 2006. Active deformation within the Zagros Mountains deduced from GPS measurements, Journal of Geological Society of London: 163,143–148.

Iranian Seismological Center (ISC). 2016. http://irsc.ut.ac.ir/currentearthq.php?lang=fa .

Jafargandomi, A., Fatemi Aghda, S. M., Suzuki, S., Nakamura, T. 2004. Strong ground motions of the 2003 Bam Earthquake, Southeast of Iran (Mw = 6:5), Bulletin of the Earthquake Research Institute: 79, 47–57.

Jankowski, P. 1995. Integrating geographical information systems and multiple criteria decision-making methods. International Journal Geographical Information Science: 9, 251–273.

Jha, M. K., Chowdary, V. M., Chowdhury, A. 2010. Groundwater assessment in Salboni Block, West Bengal (India) using remote sensing, geographical information system and multi-criteria decision analysis techniques. Hydrogeological Journal: 18, 1713–1728.

Jha, M. K., Chowdhury, A., Chowdary, V. M., Peiffer, S. 2007. Groundwater management and development by integrated remote sensing and geographic information systems: prospects and constraints. Water Resources Management: 21, 427–467.

Kamel, A. F. 1991. Analysis of structural lineaments and their effect on the distribution of ring complexes in Southeastern Desert, Egypt. Journal of African Earth Sciences: 13, 193–199.

Kanamori, H. 1977. The energy release in great earthquakes. Journal Geophysical Research: 82, 2981–2987.

Karimpour, M. H., Stern, C. R., Farmer, L., Saadat, S., Malekezadeh, A. 2011. Review of age, Rb–Sr geochemistry and petrogenesis of Jurassic to Quaternary igneous rocks in Lut Block, Eastern Iran. Geopersia: 1, 19–36.

Kienzle, A., Hannich, D., Wirth, W., Ehret, D., Rohn, J., Ciugudean, V., Czurda, K. 2006. A GIS-based study of earthquake hazard as a tool for the microzonation of Bucharest. Engeering Geology: 87, 13–32.

Kostrov, B. 1974. Seismic moment and energy of earthquakes and seismic flow of rock. Izv. Acad. Science. USSR. Physics of the Solid Earth (Engl. Trasl.): 1, 23–40.

Kramer, S. L. 1996. Geotechnical Earthquake Engineering. (1stedn), Prentice-Hall, Inc. Upper Saddle River, New Jersey 07458, USA.

Lee, S., Song, K. Y., Kim, Y., Park, I. 2012. Regional groundwater productivity potential mapping using a geographic information system (GIS) based artificial neural network model. Hydrogeological Journal: 20,1511–15 27.

Machiwal, D., Jha, M. K., Mal, B. C. 2011. Assessment of groundwater potential in a semi-arid region of India using remote sensing, GIS and MCDM techniques. Water Resources Management: 25, 1359–1386.

Mahdi, T., Mahdi, A. 2013. Reconstruction and retrofitting of buildings after recent earthquakes in Iran. Procedia Engineering: 54, 127–139.

Malczewski, J. 2006. GIS-based multi-criteria decision analysis: a sur- vey of the literature, Int. Journal Geographical Information Sciences: 20, 703–726.

Malczewski, J. 1999. GIS and multi-criteria decision analysis, John Wiley, Toronto.

Markham, B. L., Barker, J. 1986. Landsat MSS and TM post-calibration dynamic ranges, exoatmospheric reflectances and at-satellite temperatures. EOSAT Landsat Tech Notes: 1, 3–8.

Masoud, A., Koike, K. 2006. Tectonic architecture through Landsat-7 ETM?/SRTM DEM-derived lineaments and relationship to the hydrogeologic setting in Siwa region, NW Egypt. Journal of African Earth Sciences: 45:467–477.

McCall, G. J. H. 1997. The geotectonic history of the Makran and adjacent areas of southern Iran. Journal of Asian Earth Sciences: 15, 517–531.

McQuarrie, N., Stock, J. M., Verdel, C., Wernicke, B.P. 2003. Cenozoic evolution of Neotethys and implications for the causes of plate motions. Geophysical Research Letters: 30, 2036–2047.

Mohammady, M., Pourghasemi, H. R., Pradhan, B. 2012. Landslide susceptibility mapping at Golestan Province, Iran: a comparison between frequency ratio, Dempster–Shafer, and weights-of-evidencemodels. Journal of Asian Earth Sciences: 61, 221–236.

Mohanty, W. K., Walling, M. Y. 2008. First order seismic microzonation of Haldia, Bengal Basin (India) using a GIS platform. Pure and Applied Geophysics: 165, 1325–1350.

Moradi, M., Delavar, M. R., Moshiri, B. 2013. Sensitivity analysis of ordered weighted averaging operator in earthquake vulnerabilit vulnerability assessment, in: Proceedings of SMPR 2013 Conference, 5–8 October 2013, Tehran, Iran: 277–282.

Moustafa, S. S. R., Al-Arifi Jafri, M. K., Naeem, M., Alawadi, E. A., Metwaly, M. A. 2016. First level seismic microzonation map of Al-Madinah province, western Saudi Arabia using the geographic information system approach, Environmental Earth Sciences: 75, 251–271.

Nath, S. K., Thingbaijam, K. K. S., Raj, A. 2008. Earthquake hazard in Northeast India—a seismic microzonation approach with typical case studies from Sikkim Himalaya and Guwahati city. Journal Earth System Sciences: 117, 809–831.

Nath, S. K. 2004. Seismic hazard mapping and microzonation in the Sikkim Himalaya through GIS integration of side effects and strong ground motion attributes. Natural Hazards: 31, 319–342.

Nath, S. K. 2005. An initial model of seismic microzonation of Sikkim Himalaya through thematic mapping and GIS integration of geological and strong motion features. Journal of Asian Earth Sciences: 25, 329–343.

Nath, S. K., Thingbaijam, K. K. S. 2009. Seismic hazard assessment—a holistic microzonation approach. Natural Hazards and Earth System Sciences: 9, 1445–1459.

National Report of the Islamic Republic of Iran on Disaster Reduction. 2014. World Conference on Disaster Reduction, 18–22 January 2005, Kobe, Hyogo, Japan. 2005. available at: http://www.unisdr.org/2005/mdgs-drr/national-reports/Iran-report.pdf (last access: 24 July 2014).

Nefeslioglu, H. A., Sezer, E. A., Gokceoglu, C., Ayas, Z. 2013. A Modified Analytical Hierarchy Process (M-AHP) approach for decision support systems in natural hazard assessments, Computer and GeoSciences: 59, 1–8.

Pal, I., Nath, S. K., Shukla, K., Pal, D. K., Raj, A., Thingbaijam, K., Bansal, B. 2008.

Earthquake hazard zonation of Sikkim Himalaya using a GIS platform. Natural Hazards: 45, 333–377.

Panahi, M., Rezaie, F., Meshkani, S. A. 2014. Seismic vulnerability assessment of school buildings in Tehran city based on AHP and GIS. Natural Hazards and Earth System Sciences: 14, 969–979.

Papadimitriou, A. G., Antoniou, A. A., Bouckovalas, G. D., Marinos, P. G. 2008. Methodology for automated GIS-aided seismic micro- zonation studies. Computer and Geotechnics: 35, 505–523.

Parolai, S., Grunthal, G., Wahlstrom, R. 2007. Site-specific response spectra from the combination of microzonation with probabilistic seismic hazard assessment-an example for the Cologne (Germany) area. Soil Dynamics and Earthquake Engineering: 27, 49–59.

Pourghasemi, H. R., Moradi, H. R., Fatemi Aghda, S. M. 2013. Landslide susceptibility mapping by binary logistic regression, analytical Arab Journal GeoScience hierarchy process, and statistical index models and assessment of their performances. Natural Hazards: 69, 749–779.

Pourghasemi, H. R., Moradi, H. R., Fatemi Aghda, S. M., Gokceoglu, C., Pradhan, B. 2012. GIS-based landslide susceptibility mapping with probabilistic likelihood ratio and spatial multi-criteria evaluation models (North of Tehran, Iran). Arabian Journal of GeoSciences: 7, 1857–1878.

Pourtaghi, Z. S., Pourghasemi, H. R. 2014. GIS-based groundwater spring potential assessment and mapping in the Birjand Township, southern Khorasan Province, Iran. Hydrogeological Journal: 22, 643–662.

Pradhan, B. 2009. Groundwater potential zonation for basaltic watersheds using satellite remote sensing data and GIS techniques. Central European Journal of GeoSciences: 1, 120–129.

Pradhan, B. 2013. A comparative study on the predictive ability of the decision tree, support vector machine and neuro-fuzzy models in landslide susceptibility mapping using GIS. Computer and GeoSciences: 51, 350–365.

Pradhan, B., Pirasteh, S. 2010. Comparison between prediction capabilities of neural network and fuzzy logic techniques for landslide susceptibility mapping. Disaster Advances: 3, 26–34.

Pradhan, B., Youssef, A. M. 2010. Manifestation of remote sensing data and GIS for landslide hazard analysis using spatial-based statistical models. Arabian Journal of GeoSciences: 3, 319–326.

Pradhan, B., Singh, R. P., Buchroithner, M. F. 2006. Estimation of stress and its use in evaluation of landslide prone regions using remote sensing data. Advances on Space Research: 37, 698–709.

Quadrio, B., Ambrosanio, M., Ioannilli, M. 2015. A GIS-based tool for reliability assessment of seismic microzonation studies according to Italian instructions and criteria. Engineering Geology for Society and Territory: 5, 1123–1126.

Ramezani, J., Tucker, R. D. 2003. The Saghand region, central Iran: U–Pb geochronology, petrogenesis and implications for Gondwana tectonics. American Journal Science: 303, 622–665.

Rashed, T., Weeks, J. 2003. Assessing vulnerability to earthquake hazards through spatial multi-criteria analysis of urban areas. International Journal Geographical Information Sciences: 17, 547–576.

Regmi, A. D., Devkota, K. C., Yoshida, K., Pradhan, B., Pourghasemi, H. R., Kumamoto, T., Akgun, A. 2013. Application of frequency ratio, statistical index, and weights-of-evidence models and their comparison in landslide susceptibility mapping in Central Nepal Himalaya. Arabian Journal of GeoSciences: 7, 725–742.

Saaty, T. L. 1988. What is the analytic hierarchy process? Springer, Berlin, Heidelberg: pp.109–121.

Saaty, T. L. 1990. How to make a decision: the analytic hierarchy process. European Journal of Operational Research: 48, 9–26.

Saaty, T. L. 1994. How to make a decision: the analytic hierarchy process. Interfaces: 24, 19–43.

Saaty, T. L. 2004. Decision making with the analytic hierarchy process. International Journal of Services Sciences: 1, 83–98.

Saccani, E., Delavari, M., Beccaluva, L., Amini, S. 2010. Petrological and geochemical constraints on the origin of the Nehbandan ophiolitic complex (eastern Iran): Implication for the evolution of the Sistan Ocean. Lithos: 117, 209–228.

Schmidtlein, M. C., Deutsch, R. C., Piegorsch, W. W., Cutter, S. L. 2008. A sensitivity analysis of the Social Vulnerability Index. Risk Analysis: 28, 1099–1114.

Sella, G. F., Dixon, T. H., Mao, A. 2002. REVEL: a model for recent plate velocities from space geodesy. Journal Geo Res: 107, 11–30.

Şengör, A. M. C., Altlner, D., Cin, A., Ustaomer, T., Hsu, K. J. 1988. Origin and Assembly of the Tethyside Orogenic Collage at the Expense of Gondwana Land. In: Audley- Charles MG, Hallam AE. (Eds.), Gondwana and Tethys. Geological Society of London Special Publication. Blackwell, Oxford: pp.119–181.

Şengör, A. M. C., Natal'in, B. A. 1996. Paleotectonics of Asia: fragments of a synthesis. In: Yin, A., Harrison, M. (Eds.), The Tectonic Evolution of Asia. Cambridge University Press. Cambridge: pp.486–640.

Servi, M. 2004. Assessment of vulnerability to earthquake hazards using spatial multi-criteria analysis: Odunpazari, Eskisehir case study. MS thesis, Middle East Technical University, Turkey: 94.

Srivastava, P. K., Bhattacharya, A. 2006. Groundwater assessment through an integrated approach using remote sensing, GIS and resistivity techniques: a case study from a hard rock terrain. International Journal Remote Sensing: 27, 4599–4620.

Stöcklin, J. 1968. Structural history and tectonics of Iran: a review. American Association of Petroleum Geologists Bulletin: 52, 1229–1258.

Suárez-Vega, R., Santos-Peñate, D. R., Dorta-González, P., Rodríguez-Díaz, M. 2011. A multi-criteria GIS based procedure to solve a network competitive location problem. Applied Geography: 31, 282–291.

Takin, M. 1972. Iranian geology and continental drift in the Middle East, Nature: 235, 147–150.

Tirrul, R., Bell, I. R., Griffis, R. J., Camp, V. E. 1983. The Sistan suture zone of eastern Iran. Geological Society of America Bulletin: 94, 134–150.

Turk, T., Gumusay, U., Tatar, O. 2012. Creating infrastructure for seismic microzonation by geographical information systems (GIS): a case study in the North Anatolian Fault Zone (NAFZ). Computer and GeoSciences: 43, 167–176.

USGS. Hazards. 2014. http://earthquake.usgs.gov/hazards ./

Vernant, P. h., Nilforoushan, F., Hatzfeld, D., Abbassi, M. R., Vigny, C., Masson, F., Nankali, H., Martinod, J., Ashtiani, A., Bayer, R., Tavakoli, F., Chéry, J. 2004. Present-day crustal deformation and plate kinematics in the Middle East constrained by GPS measurements in Iran and northern Oman. Geo Journal Int: 157, 381–398.

Walker, R., Jackson, J. 2002. Offset and evolution of the Gowk fault, S.E. Iran: a major intra-continental strike–slip system. Journal of Structural Geology: 24, 1677–1698.

Wang, F. 2014. Reducing geo-disasters for improving the relationships between geoenvironment and society. Geoenvironmental Disasters: 1, 3. DOI: 10.1186/s40677-014-0003-4

Wellman, H. W. 1966. Active wrench faults of Iran, Afghanistan and Pakistan. Geologische Rundschau: 18, 217–234.

Yalcin, A. 2008. GIS-based landslide susceptibility mapping using analytical hierarchy process and bivariate statistics in Ardesen (Turkey): comparisons of results and confirmations. Catena: 72, 1–12.

Zare, M., Pourghasemi, H. R., Vafakhah, M., Pradhan, B. 2013. Landslide susceptibility mapping at Vaz watershed (Iran) using an artificial neural networkmodel: a comparison betweenmulti-layer perceptron (MLP) and radial basic function (RBF) algorithms. Arabian Journal of GeoSciences: 6, 2873–2888.

Zarrinkoub, M. H., Chung, S. L., Chiu, H. Y., Mohammadi, S., Khatib, M., Lin, I. J. 2010. Zircon U–Pb age and geochemical constraints from the northern Sistan suture zone on the Neotethyan magmatic and tectonic evolution in eastern Iran. Abstract to GSA Conference on “Tectonic Crossroads: Evolving Orogens in Eurasia–Africa–Arabia”, 4–8.520. Ankara, Turkey.